Supporting Information

Controllable synthesis of highly uniform flower-like hierarchical carbon nanospheres and its application in high performance lithium-sulfur batteries

Daying Guo, Xi'an Chen*, Huifang Wei, Menglan Liu, Feng Ding, Zhi Yang, Keqin Yang, Shun Wang, Xiangju Xu, Shaoming Huang*

Key Laboratory of Carbon Materials of Zhejiang Province, College of Chemistry and Materials Engineering, Wenzhou University, Wenzhou 325035, P.R. China. E-mail: xianchen@wzu.edu.cn (Xi'an Chen), smhuang@wzu.edu.cn (Shaoming Huang)

Tel. and fax: +86 577 88373017

The preparation and adsorption of Lithium Polysulfide

Lithium polysulfide (Li_2S_6) was synthesized according to the literature [1]. The adsorption ability of the FCNS2-750, FCNS2-800, FCNS2-900, FCNS2-1000 and NFCNS2-900 on lithium polysulfide was investigated by UV-Vis spectroscopy (UV1800 spectrophotometer Shimadzu). Typically, 50 mg of each carbon host was placed in 5 mL of Li_2S_6 solution (5 mM), and the mixture was stirred for 30 min.

Electrode preparation, Cell assembling and electrochemical measurements

The different FHCS/S composite was mixed with carbon black and polyvinylidene fluoride (PVDF) at a mass ratio of 80:10:10 with N-methyl pyrrolidone (NMP) as a dispersant. Electrode paste was coated on aluminum foil with different specifications and was cutting into a film disk of 14 mm in diameter. The as-obtained film disk was dried in a vacuum oven at 60 °C for 12 h. CR2025-type coin cells were assembled by sandwiching FCNS2-900 or NFCNS2-900 coated celgard @ separator between the film disk and a lithium metal foil in a high-purity argon-filled glove box. 1 wt% anhydrous lithium nitrate (analytical grade) and 1 M $LiN(CF_3SO_2)_2$ (LiTFSI) in a mixed solvent of 1, 3-dioxolane (DOL) and dimethyl ether (DME) at a volume ratio

of 1:1 were used as the electrolyte, purchased from Fosai New Material Co., Ltd (Suzhou). The mass ratio of the electrolyte to sulfur is 40~50. The flexible freestanding FCNS2-900 or NFCNS2-900 coated celgard@ separator film was prepared by coating FCNS or NFCNS slurry composed of FCNS2-900 or NFCNS2-900 and PVDF with the weight ratio of 9:1 on the separator. After drying at 50 °C under vacuum, a large piece of flexible FCNS2-900 or NFCNS2-900 coated celgard separator was obtained and used as interlayer. The mass loading of FCNS2-900 or NFCNS2-900 in the interlayer is around 0.3 mg cm^{-2} [2]. Galvanostatic charge/discharge tests were conducted to evaluate the electrochemical capacity and cycle stability of the electrodes on the basis of the active sulfur at current densities of 0.2 C, 0.5 C, 1 C, 2 C, 3 C, 5 C (1 C = 1675 mA g^{-1}) from 1.5 to 3.0 V using a LANHE instrument (Wuhan Land electronics Co., Ltd China). All the capacities were calculated based on the weight of sulfur in the cathodes other than mentioned specially. CV data were recorded on a CHI660e electrochemical workstation (Shanghai Chenhua) between 1.6 and 2.8 V to characterize the redox behavior and the kinetic reversibility of the cell. The AC impedance was measured with fresh cells at the open circuit potential, which was also carried out using a CHI 660e electrochemical workstation. The AC amplitude was 5 mV and the frequency ranged from 100 kHz to 0.01 Hz.

Materials characterization

The content of sulfur loading was confirmed using a TG/DTA thermogravimetric analyzer (Diamond PE) under an N_2 atmosphere at a heating rate of 10 °C min^{-1} from room temperature to 600 °C, with a flow rate of 200 mL min^{-1}. SEM images were obtained with a Nova NanoSEM 200 scanning electron microscope (FEI, Inc.). TEM, HRTEM images were recorded with a JEOL2100 instrument. Powder XRD was carried on a Bruker D8 Advance X-ray diffractometer using CuKa radiation (λ= 0.15418 nm) at a scanning rate of 4ºmin^{-1} in the 2θ range from 10º to 80º. X-ray photoelectron spectroscopy (XPS) measurements were conducted with an ultrahigh vacuum setup, equipped with a monochromatic Al Ka X-ray source and a high resolution Thermo ESCALAB 250 analyzer. Raman spectra were collected on a

Labram-010 microscopic confocal Raman spectrometer with a 633 nm laser excitation. Specific surface area, pore volume and pore size distribution were determined by the BET method on a Micromeritics ASAP 2020 instrument.

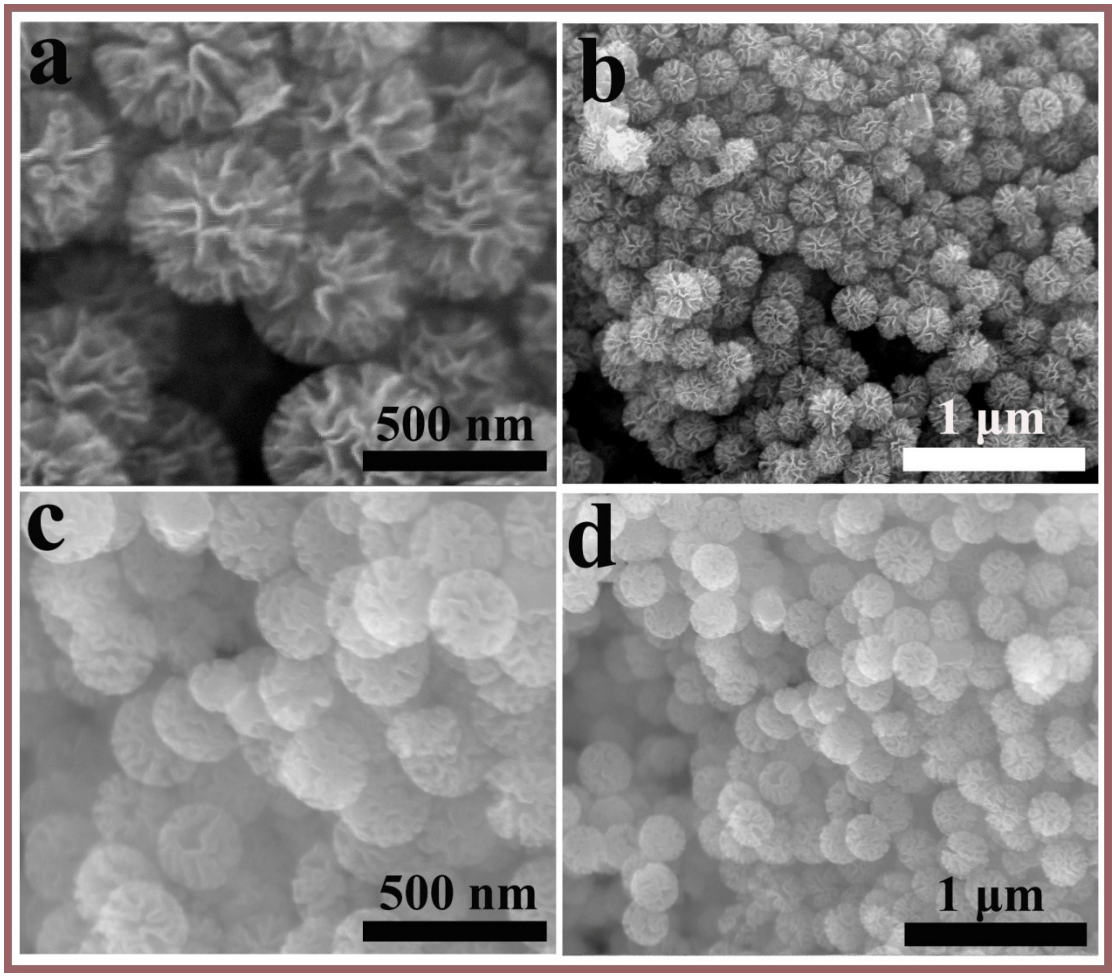

Fig. S1 SEM images of FCNS1-900(a, b) and FCNS3-900 (c, d).

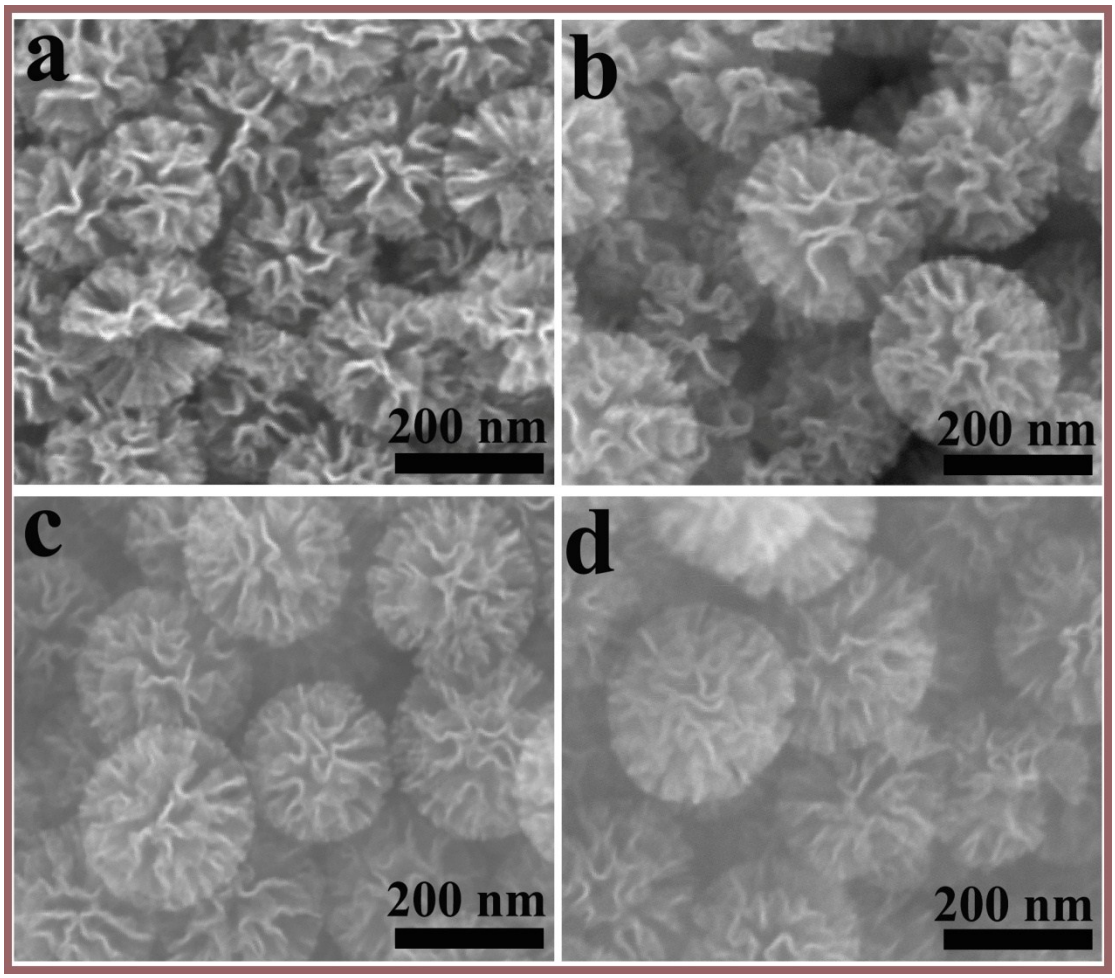

Fig. S2 SEM images of FCNS2-750 (a), FCNS2-800 (b), FCNS2-900 (c), FCNS2-1000 (d).

Table S1 Specific surface area (SSA) and pore volume of FCNS2-750, FCNS2-800, FCNS2-900 and FCNS2-1000 evaluated by the Brunauer-Emmett-Teller (BET) and Density Functional Theory (DFT) method, respectively.

Samples	**SSA ($m^2 g^{-1}$)**	**Pore Volume ($cm^3 g^{-1}$)**
FCNS2-750	1104	1.33
FCNS2-800	1148	1.86
FCNS2-900	1151	1.95
FCNS2-1000	1081	1.74

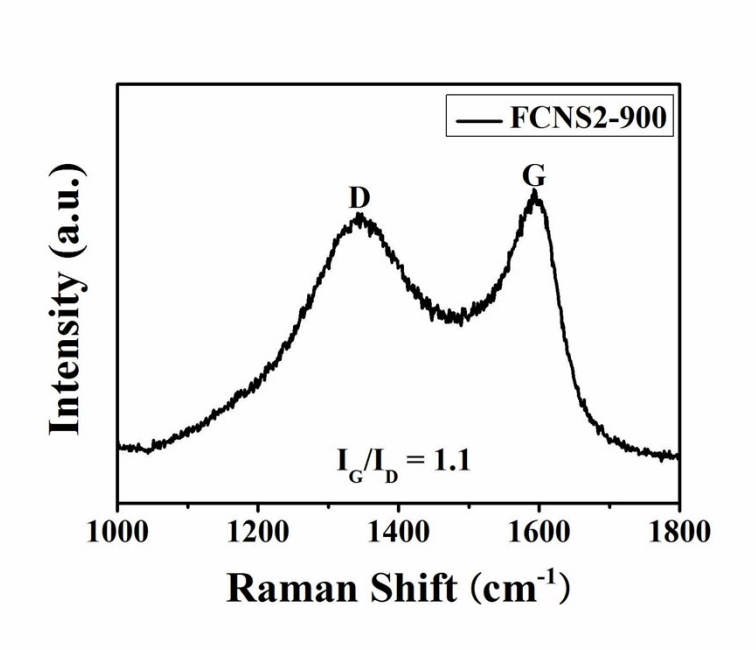

Fig. S3 Raman spectrum of FCNS2-900.

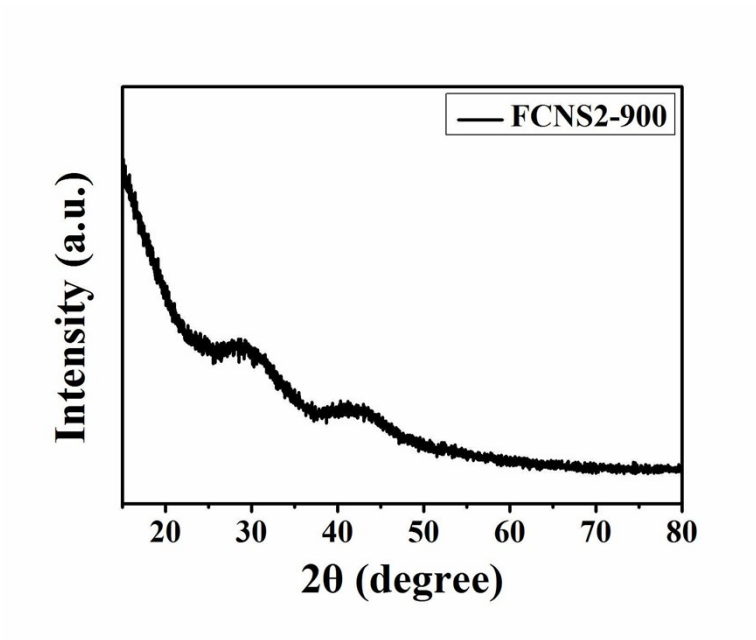

Fig. S4 XRD pattern of FCNS2-900

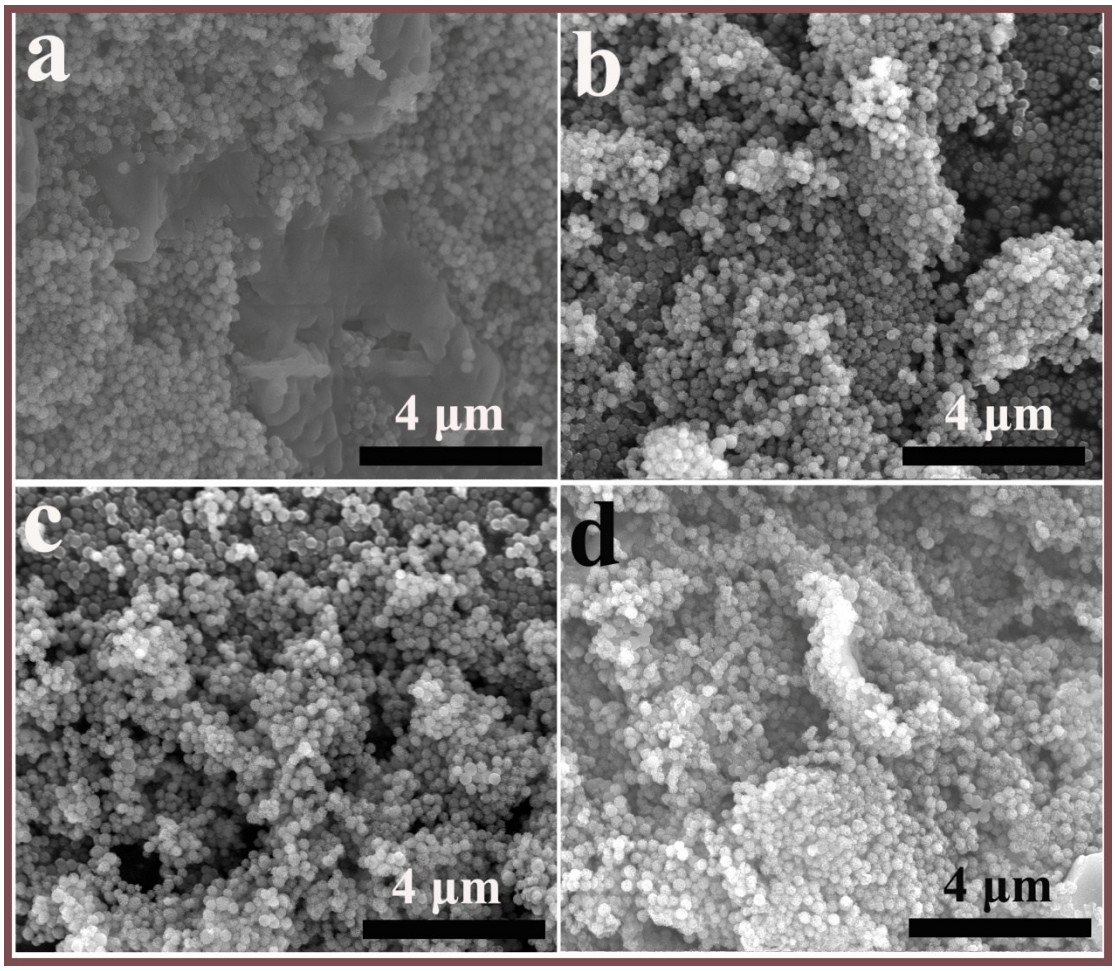

Fig. S5 SEM images ofFCNS2-750/S81% (a), FCNS2-800/S81% (b), FCNS2-900/S81% (c) and (d) FCNS2-1000/S81%.

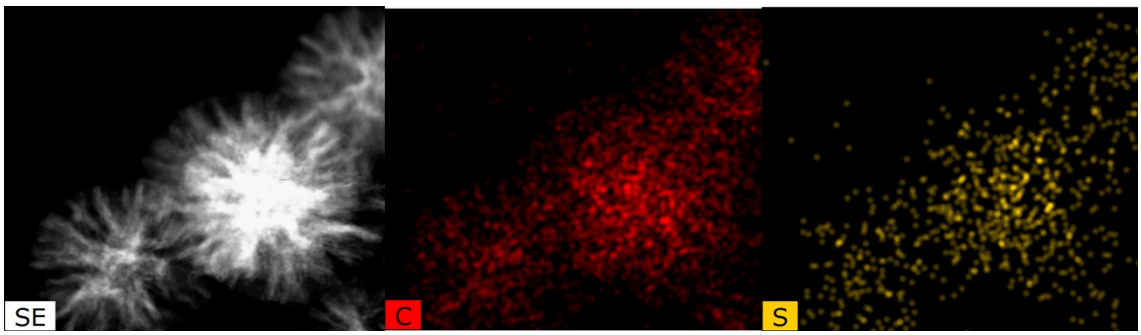

Fig. S6 The STEM-EDS elemental mapping of FCNS2-900/S81%

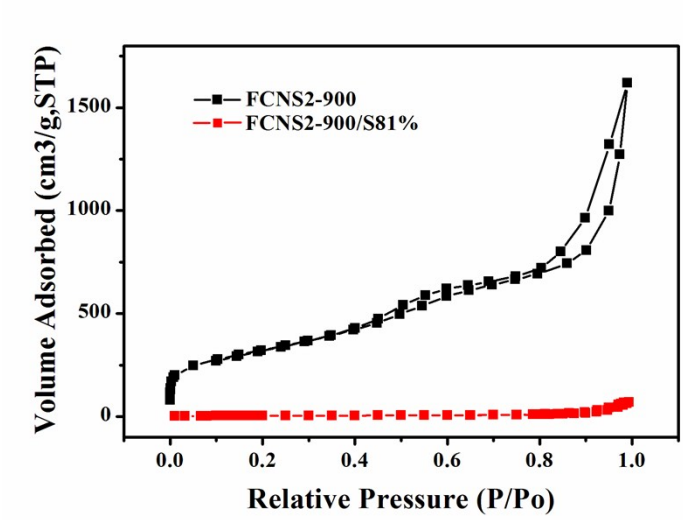

Fig. S7 The nitrogen adsorption and desorption isotherms of FCNS2-900 and FCNS2-900/S81%

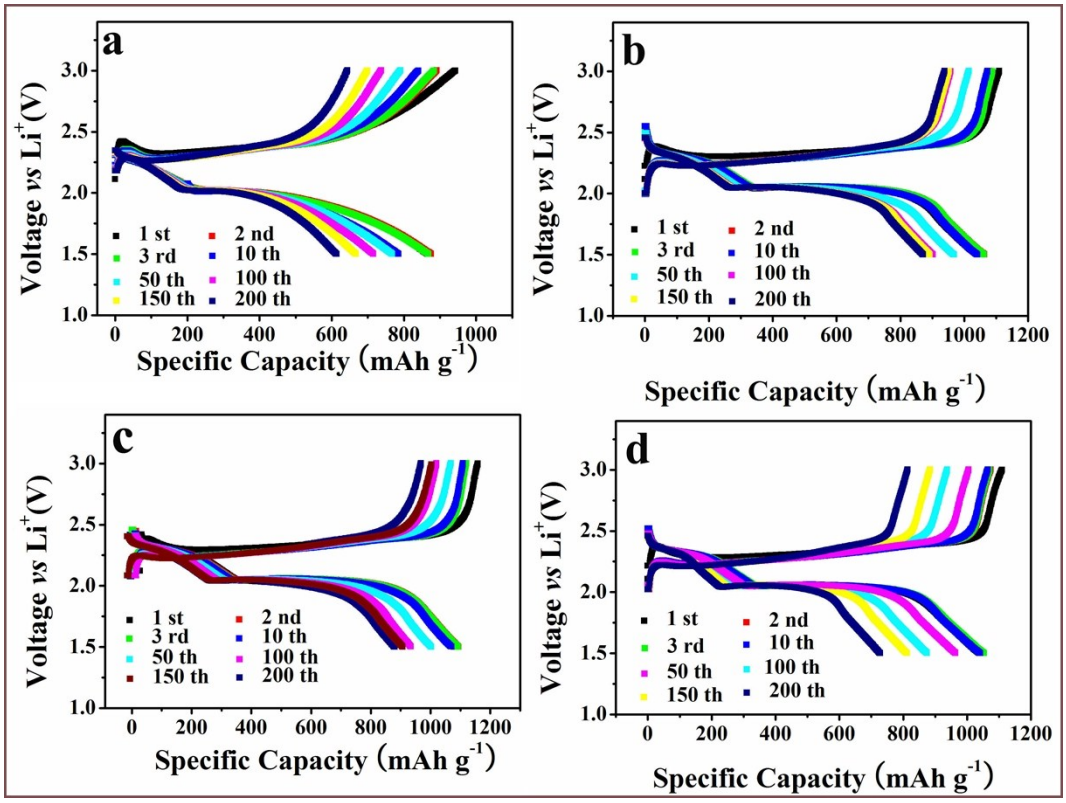

Fig. S8 a, b, c, d) discharge-charge profiles of FCNS2-750/S81%, FCNS2-800/S81%, FCNS2-900/S81%, and FCNS2-1000/S81%, respectively.

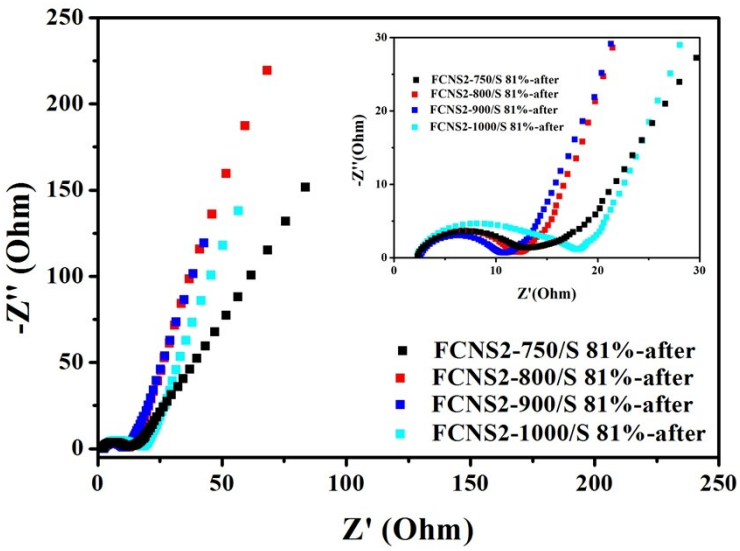

Fig. S9 The Nyquist plots of the cells with the cells after cycling.

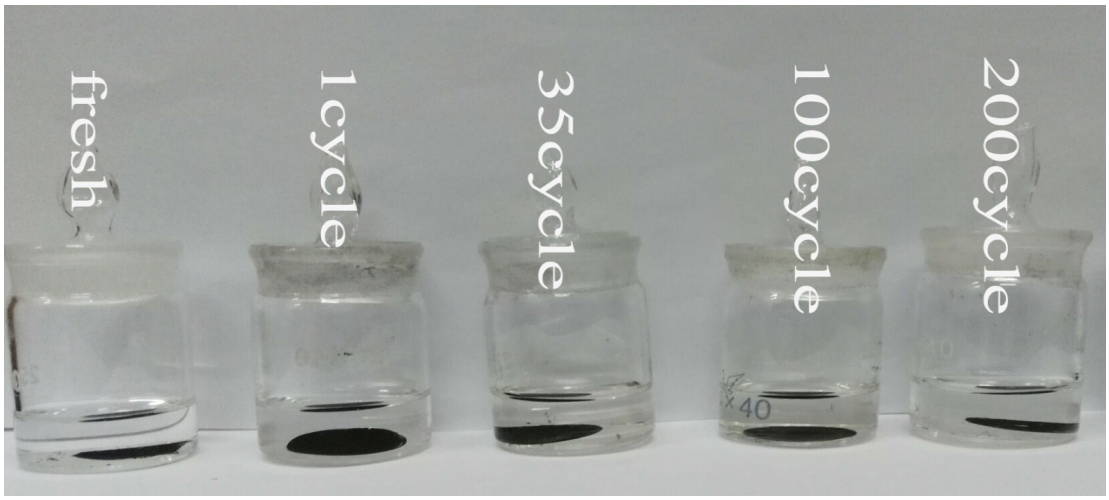

Fig. S10 Typical colors of electrolyte for the FCNS2-900/S81% cathode after various cycles in sealed vials. The solution obtained by soaking the cycled cathodes (discharge state) in a mixture of DOl/DME (1:1, vol).

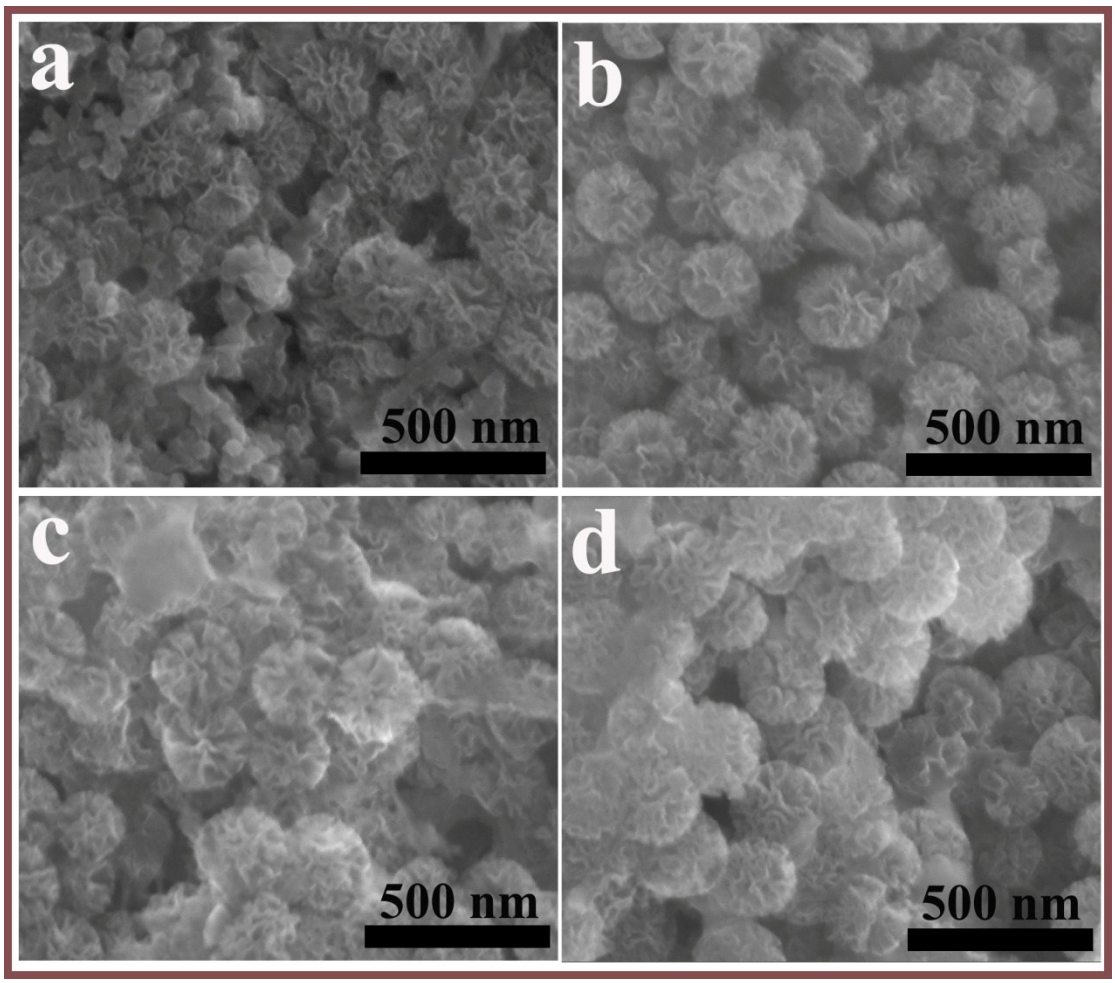

Fig. S11 SEM images of FCNS2-900/S81% cathode: a) fresh; b) after 35 cycles; c) after 100 cycles; d) after 200 cycles.

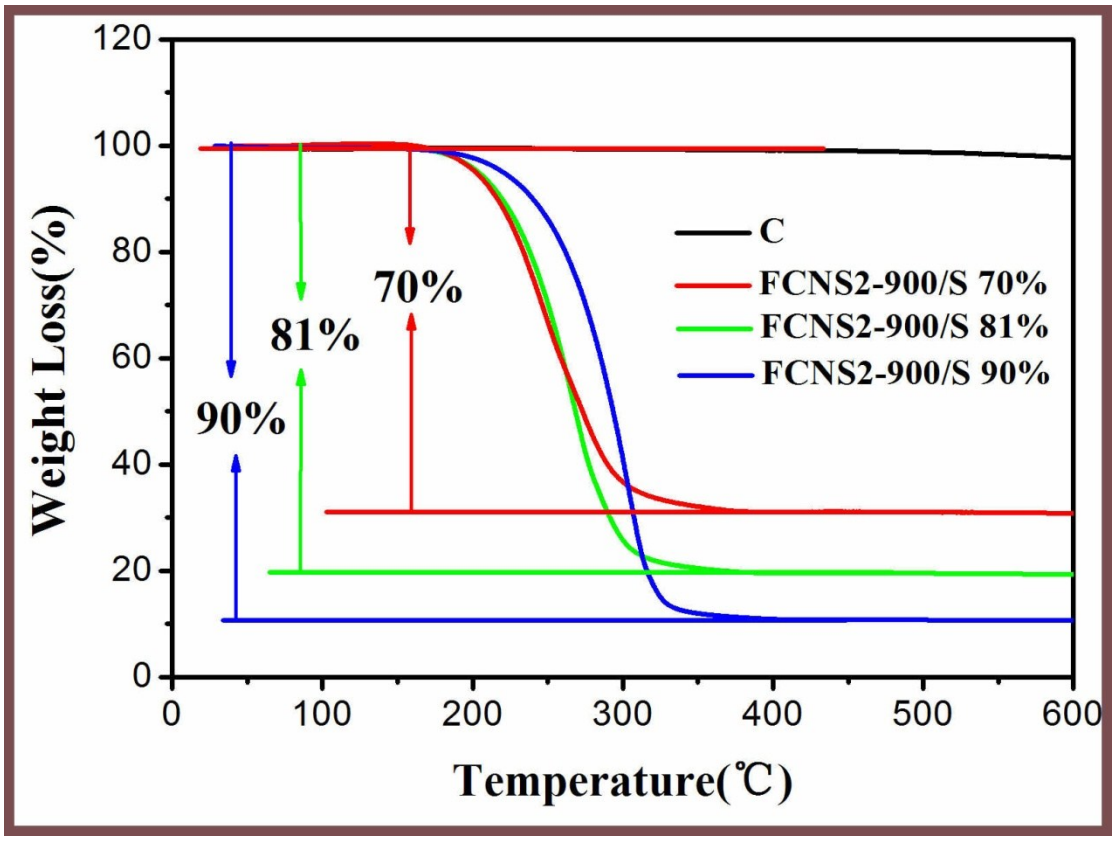

Fig. S12 FCNS2-900/S 70%, FCNS2-900/S 81% and FNCNS2-900/S 90% of TGA curves.

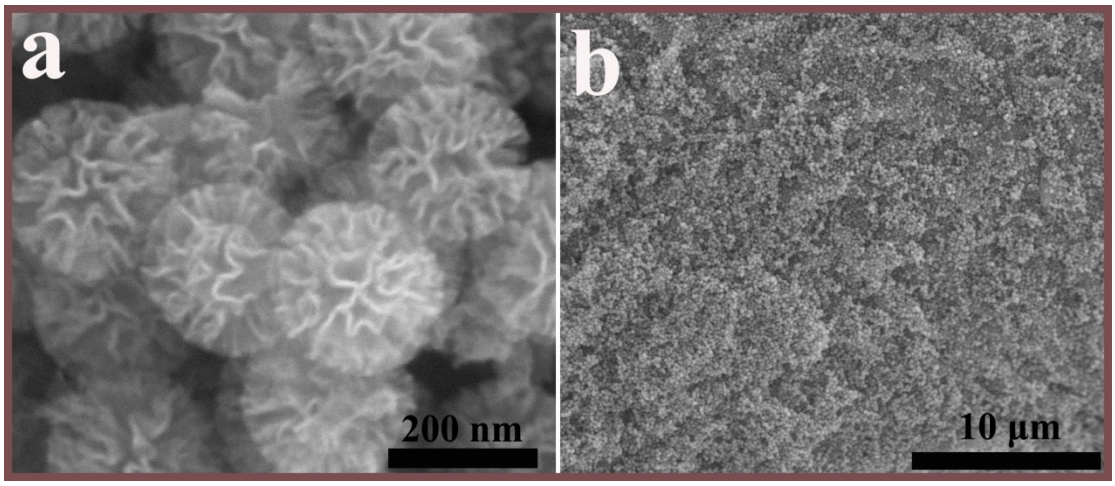

Fig. S13 SEM images of FNCNS2-900

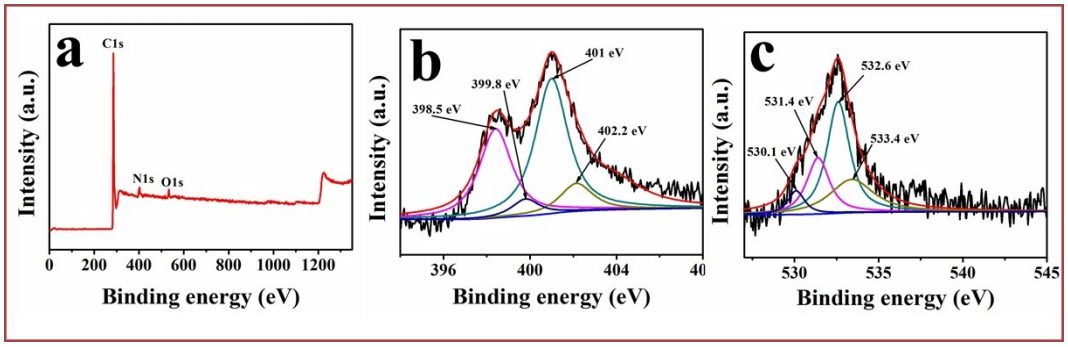

Fig. S14 XPS survey spectrum (a); high resolution XPS of N1s (b); high resolution XPS of O1s for NFCNS2-900

Table S2 The content of C, N and O in the NFCNS2-900 sample

Sample Name	C	N	O
NFCNS2-900	91.95%	5.68%	2.37%

Table S3 The analysis results of N1s XPS

Sample Name	Total N	pyridinic-N	pyrrolic-N	graphitic-N	oxygen-N
NFCNS2-900	5.68%	1.91%	0.30%	2.88%	0.59%

Table S4 The analysis results of O1s XPS

Sample Name	Total oxygen	C=O	C-O	C-O-C	O-H
NFCNS2-900	2.37%	0.17%	0.59%	1.25%	0.36%

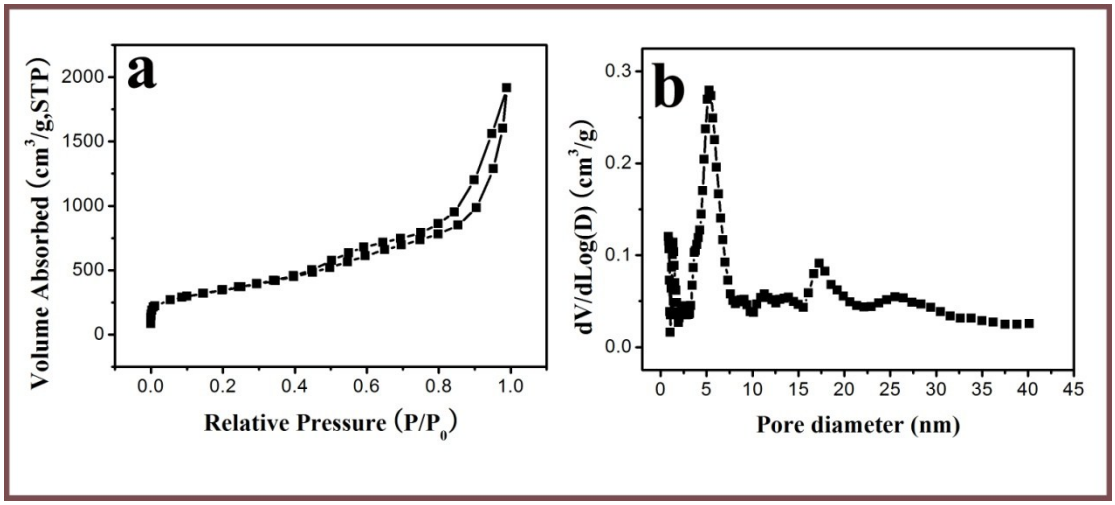

Fig. S15 a, b) Nitrogen adsorption-desorption curves isotherms and pore size distribution plots obtained using the DFT method of the NFCNS2-900

Table S5 Specific surface area and pore volume of FCNS2-900 and NFCNS2-900 evaluated by the Brunauer-Emmett-Teller (BET) and Density Functional Theory (DFT) method, respectively.

Samples	**SSA (m^2 g^{-1})**	**Pore Volume (cm^3 g^{-1})**
FCNS2-900	1151	1.95
NFCNS2-900	1229	2.33

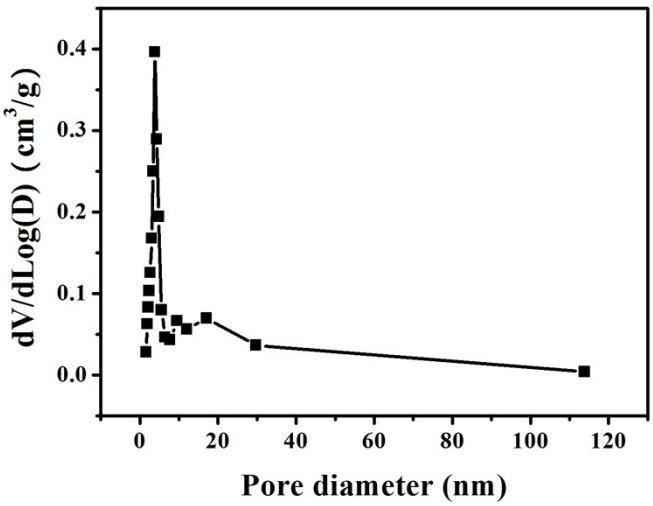

Fig. S16 The pore size distribution of NFCNS2-900 based on the BJH method.

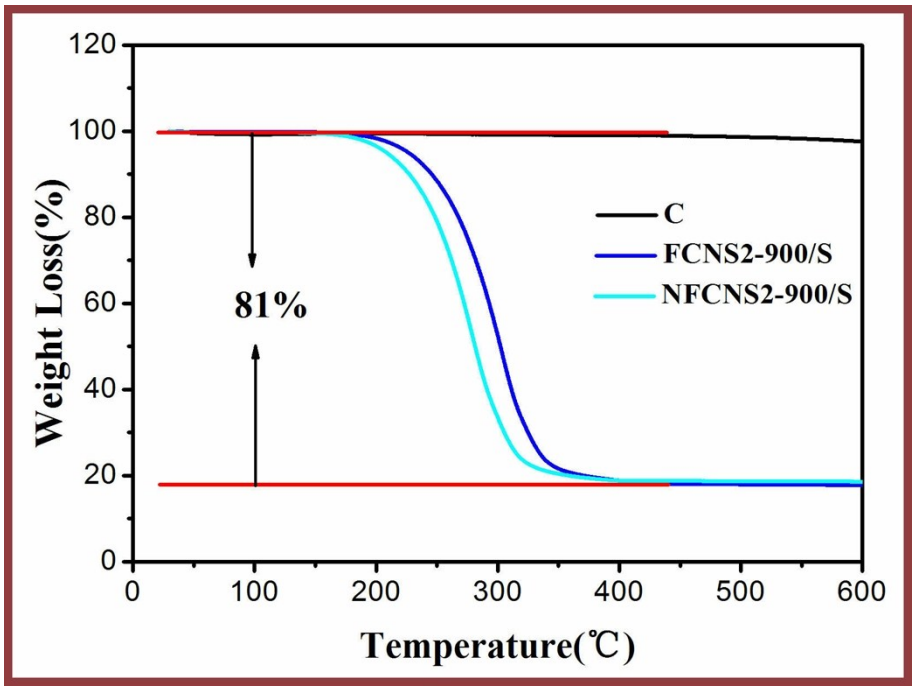

Fig. S17 FCNS2-900/S and NFCNS2-900/S of TGA curves.

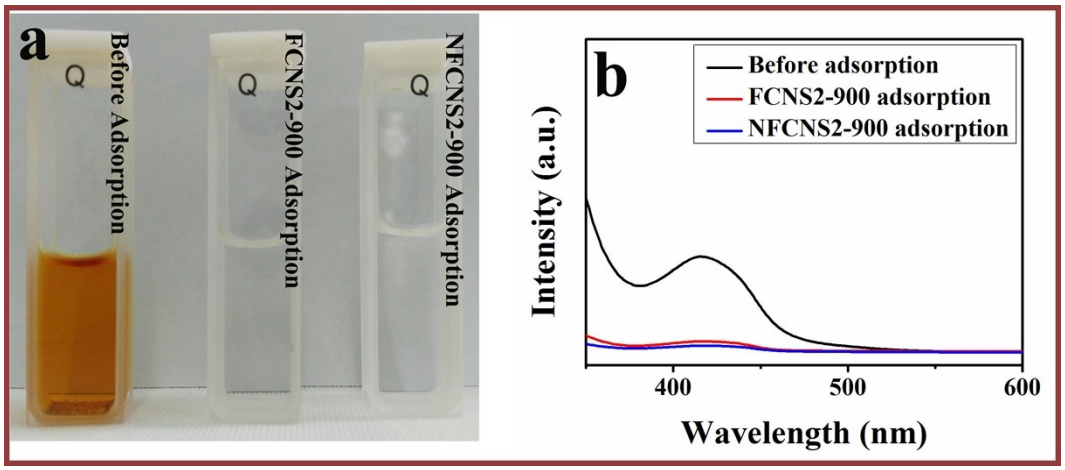

Fig. S18 a) Associated color changes of a polysulfide solution before and after exposure to the FCNS2-900 and NFCNS2-900, respectively adsorbents. (b) UV-vis spectra of a polysulfide solution before and after exposure to the FCNS2-900 and FNCNS2-900, respectively adsorbents.

Table S6 A comparison of comprehensive performance between this work and some other Li-S cells based on the carbon materials reported in previous literature.

Cathode materials (sulfur host)	Sulfur Loading	Capacity(calculate based on the sulfur)	stability (decay rate per cycle)	Refs.
Tailoring Porosity in Carbon Nanospheres	70%	1015 0.2 C 920 0.5C 875 1C	0.1% per cycle at 1C	3
Hierarchical Porous Carbon nanosheets	74%	1370 0.5C 1200 1C 860 5C	0.25% decay for 100 cycles at 1 C	4
Hierarchical Vine-Tree-Like Carbon Nanotube Architectures	60%	1418 0.5C (initial) 997 3C 630 4C	0.08% decay for 450 cycles at 1 C	5
Polydopamine-Coated, Nitrogen-Doped, Hollow Carbon	55%	1070 0.2C 740 0.6C	0.1% decay per cycle for 150 cycles at 0.2 C	5
Graphene/Sulfur Hybrid Nanosheets	68%	1200 0.2 C 700 2C 400 5C	0.5% decay for 70 cycles at 0.5 C	7
Pie-like electrode design	72.3%	1,113 0.2 C 801 0.5C 688 1C 363 2C	0.1% decay per cycle at 0.1 C	8
ultrahigh-surface-area hollow carbon nanospheres	67%	1240 0.2C 1026 0.5C 965 1 C	0.07% decay per cycle at 0.5C	9

		655 2C		
Nitrogen-Doped Hollow Carbon Nanospheres	85%	1139 0.2C 920 0.5C 720 1C 250 2C	0.12% decay for 200 cycles at 0.2 C	10
Hierarchical carbon nanocages	79.8%	1214 0.2 A g^{-1} 580 3 A g^{-1}	0.16 % decay for 300 cycles at 1 A g^{-1}	11
h-CNT/S/ZrO_2 composite cathode	45.2%	4c 1000 10c 850	0.11% decay per cycle at 0.5 C	12
Nitrogen and Sulfur Dual-Doped Carbon	70%	1370 0.05c 1280 0.2C, 1135 0.5C 830 2C	0.052% decay per cycle for 1000 cycles at 0.5 C	13
Multichannel Carbon Nanofiber	80%	1351 at 0.2 C 847 at 5C	0.07% decay per cycle for 300 cycles at 0.2C	14
Three-dimensional porous carbon	90%	1382 0.5C 1242 1C 1115 2 C	0.039% decay for 1000 cycles at 2 C	15
Graphitic carbon nanocage	77%	1024 0.5C 900 1C 875 2C 765 5C	0.0215% for 1000 cycles decay at 1 C	16
Incorporating Sulfur Inside the Pores of Carbons by An Electrolysis Approach	70%	1068 0.5C 869 1 C 725 2C 652 4C	0.08 % decay for 500 cycles at 0.5 C	*17*
Highly Crumpled Nitrogen-Doped Graphene Sheets	80%	1100 0.2C 1000 0.5C 950 1C	0.08% decay at 1.17 mA cm^{-2}	*2*
Si/SiO_2@Hierarchical Porous Carbon Spheres	69.6 %	1230 0.1C 1002 0.5C 907 1C 730 1.5C 614 2C	0.063% decay per cycle at 2 C	18
Mesoporous Carbon Nanotube Network	60%	753 1c 701 2c 655 5c	0.093 % decay for 100 cycles	*19*
N-Doped Hollow Porous Carbon Bowls	70%;	1065 0.5C 882 1C 785 2C 600 3C 535 4C	0.053% decay for 400 cycles at 1 C	20
Hierarchical Porous Graphene	68%	887 0.1 C 656 5C	0.11% decay for 150 cycles at 0.5 C	21

N-doped flower-like carbon nanospheres	81%	1190 0.5 C 1051 1C 953 2C 901 3C 829 5C	0.03% decay per cycle at 1 C	This work
Flower-like carbon nanospheres	81%	1190 0.5 C 1070 1C 960 2C 893 3C 730 5C	0.056% decay per cycle at 1 C	This work

References:

1. Q. Sun, B. He, X.-Q. Zhang, A.-H. Lu, ACS Nano, 2015, 9, 8504-8513.
2. J. X. Song, Z. X. Yu, M. L. Gordin, D. H. Wang. Nano Lett., 2016, 16, 864-870.
3. G. He, S. Evers, X. Liang, M. Cuisinier, A. Garsuch, L. F. Nazar, ACS Nano 2013, 7, 10920-10930.
4. X. A. Chen, Z. B. Xiao, X. T. Ning, Z. Liu, Z. Yang, C. Zou, S. Wang, X. H. Chen, Y. Chen, S. M. Huang, Adv. Energy Mater. 2014, 4, 1301988.
5. M. Q. Zhao, H. J. Peng, G. L. Tian, Q. Zhang, J. Q Huang, X. B. Cheng, C. Tang, F. Wei, Adv. Mater. 2014, 26, 7051-7058
6. W. D. Zhou, X. C. Xiao, M. Cai, L. Yang, Nano Lett. 2014, 14, 5250-5256.
7. L. F. Fei, X. G. Li, W. T. Bi, Z. W. Zhuo, W. F. Wei, L. Sun, W. Lu, X. J. Wu, K. Y. Xie, C. Z. Wu, H. L. W. Chan, Y. Wang, Adv. Mater. 2015, 27, 5936-5942.
8. Z. Li, J. T. Zhang, Y. M. Chen, J. Li, X. W. Lou, Nat. Commun. 2015, 6, 8850.
9. F. Xu, Z. W. Tang, S. Q. Huang, L. Y. Chen, Y. R. Liang, W. C. Mai, H. Zhong, R. W. Fu, D. C. Wu, Nat. Commun. 2015,6:7221.
10. W. D. Zhou, C. M. Wang, Q. L. Zhang, H. D. Abruña, Y. He, J. W. Wang, S. X. Mao, X. C. Xiao, Adv. Energy Mater. 2015, 5, 1401752.
11. Z. Y. Lyu, D. Xu, L. J. Yang, R. C. Che, R. Feng, J. Zhao, Y. Li, Q. Wu, X. Z. Wang, Z. Hu. Nano Energy, 2015, 12, 657-665.
12. Y. Zhou, C. G. Zhou, Q. Y. Li, C. J. Yan, B. Han , K. S. Xia, Q. Gao, J. P. Wu, Adv. Mater. 2015, 27, 3774-3781.
13. Q. Pang, J. T. Tang, H. Huang, X. Liang, C. Hart, K. C. Tam, L. F. Nazar, Adv. Mater. 2015, 27, 6021-6028.
14. J. S. Lee, W. Kim, J. Jang, A. Manthiram, Adv. Energy Mater. 2016, 1601943.
15. G. X. Li, J. H. Sun, W. P. Hou, S. D. Jiang, Y. Huang, J. X. Geng, Nat. Commun. 2016, 7, 10601.

16. J. Zhang, C. P. Yang, Y. X. Yin, L. J. Wan, Y. G. Guo, Adv. Mater. 2016, 28, 9539-9544.
17. B. He, W. C. Li, C. Yang, S. Q.Wang, A. H. Lu, ACS Nano, 2016, 10, 1633-1639.
18. S. Rehman, S. J. Guo, Y. L. Hou, Adv. Mater. 2016, 28, 3167-3172.
19. L. Sun, D. T. Wang, Y. F. Luo, K. Wang, W. B. Kong, Y. Wu, L. Zhang, K. L. Jiang, Q. Q. Li, Y. H. Zhang, J. P. Wang, S. S. Fan. ACS Nano, 2016, 10, 1300-1308.
20. F. Pei, T. H. An, J. Zang, X. J. Zhao, X. L. Fang, M. S. Zheng, Q. F. Dong, N. F. Zheng, Adv. Energy Mater. 2016, 1502539.
21. C. Tang, B. Q. Li, Q. Zhang, L. Zhu, H. F. Wang, J. L. Shi, F. Wei, Adv. Funct. Mater. 2016, 26, 577-585.